



A new multiobjective optimization with elliptical constraints approach for nonlinear models implemented in a stainless steel cladding process

Eduardo Rivelino Luz¹ · Estevão Luiz Romão¹ · Simone Carneiro Streitenberger¹ · José Henrique Freitas Gomes¹ · Anderson Paulo de Paiva¹ · Pedro Paulo Balestrassi¹

Received: 28 September 2020 / Accepted: 28 December 2020 / Published online: 6 February 2021
© The Author(s), under exclusive licence to Springer-Verlag London Ltd. part of Springer Nature 2021

Abstract

This paper proposes a new multiobjective optimization with elliptical constraints approach for nonlinear models implemented in a cladding process of ABNT 1020 carbon steel plate using austenitic ABNT 316L stainless steel cored wire. Stainless steel stands out among the cladding materials as it allows obtaining surfaces with determined desirable characteristics from lower cost materials. This kind of process may be controlled by a relatively small number of input variables, i.e., the wire feed rate (WF), voltage (V), welding speed (WS), and the distance from the contact tip to the workpiece (N). Besides that, many outputs can be evaluated and simultaneously optimized. In the present paper, dilution (D), yield (Y), convexity index (CI), and penetration index (PI) were investigated. In order to consider the problem's multivariate nature, techniques such as factor analysis and Bonferroni's multivariate intervals were applied combined with elliptical constraints. The response variables were mathematically modeled using Poisson regression, and the obtained results were satisfactory since accurate models were achieved. The normal boundary intersection (NBI) method produced a set of viable configurations for the input variables that allows the experimenter to encounter the best system setup regarding the importance level of each response. Feasible and non-dominated solutions were found which means that the best possible scenario considering all the constraints was reached.

Keywords Cladding · Design of experiments · Multiobjective constrained optimization · Factor analysis · Simultaneous confidence intervals

1 Introduction

The use of welding as a manufacturing or maintenance process in various segments of the industry has been a milestone for its growth and strengthening. Industries in general have been constantly looking for alternatives in order to reduce costs by minimizing wear and tear in their equipment [1]. For instance, stainless steels are generally deposited on surfaces of carbon steels or low alloy steels, producing a layer with anticorrosive and resistant properties that are necessary to withstand environments subject to high corrosion. This is one of the applications of cladding [2].

Cladding process is defined as the deposition of a sufficiently thick layer of some weld metal of interest on a carbon steel or low alloy surface to make it resistant to corrosion or wear [3]. It is generally applied to extend the useful life of parts that do not have all the necessary properties for a specific application and to recover elements or materials that no longer have certain characteristics required by the process or are in a state of wear or corrosion [3–6].

The results of this process have made this application quite attractive, insofar as surfaces that are resistant to corrosive environments can be produced from common materials at a lower cost compared to the use of purely stainless steel components. It guarantees the reuse of the original material that would go for disposal, and it may result in a manufacturing cost reduction, besides making the process more sustainable [7–9]. This technique extends among the most diverse types of industries, as oil, chemical, food, agricultural, nuclear, naval, railway, and civil construction [6, 10].

✉ Eduardo Rivelino Luz
eluz7777@gmail.com

¹ Institute of Industrial Engineering and Management, Federal University of Itajubá, Itajubá, MG, Brazil

Comparing the cladding process with conventional welding applications, the main difference is the importance of the weld bead geometry. In conventional applications, high penetration is desirable to guarantee the strength of the welded joint, whereas in cladding, the desired bead geometric profile must have large widths, high reinforcements, low penetrations, and low percentages of dilution, which represents the penetration area divided by the total welded area [11, 12]. Low dilution values are desirable to maintain the chemical composition of the filler metal and, consequently, its resistance to corrosion [13–15]. According to some researchers, this is one of the main characteristics to ensure the final quality of the claddings [12, 16–18]. Then, recovering the largest area as possible with the fewest number of welding passes results in significant savings in regard to the resources, such as welding time and inputs.

However, the results of the cladding of carbon steel with stainless steel are not only limited to obtaining the desired geometric profile. The industrial environments are increasingly demanding processes capable of combining minimum quality requirements with high levels of productivity, as a way to guarantee greater results and competitiveness [19, 20].

In view of this, stainless steel stands out among the cladding materials as it allows obtaining surfaces with determined desirable characteristics from lower cost materials [21]. This brings the motivation for the objective of this paper, which involves covering an ABNT 1020 carbon steel surface using ABNT 316L stainless steel tubular wire. Among the process variables, the wire feed rate, voltage, welding speed, and the distance from the contact tip to the workpiece are commonly found in the literature as influence factors [22].

The choice to use tubular wire welding was justified by the fact that it provides consistent advantages to the objectives of this study, such as the acquisition of high deposition rates, less waste of the electrode, greater flexibility of the process, high quality of the weld, and excellent control of the fusion pool [23, 24].

Response surface methodology is used in order to optimize the responses related to the cladding process such as those considered in this work: dilution, yield, convexity index, and penetration index. Many other techniques are also applied to solve the multivariate optimization problem in this paper, for instance, normal boundary intersection, Poisson regression, simultaneous confidence intervals, and factor analysis. It is worth mentioning that these tools have been used successfully in the literature for the modeling and analysis of welding processes [6, 10–13, 25, 26]. Furthermore, the application of multivariate constraints and the Poisson regression to model the responses stands out as the main contribution of the present work as can be seen in the next section in more details.

2 Related work

Experimental research has acquired considerable importance in organizational research, mainly due to two facts. The first concerns the strength of this method of investigation in allowing the researcher to make strong statements of causality. The second fact of the importance of experimental research concerns the facility that the researcher who employs experimental projects (or designs) finds to establish cause and effect relationships, making the experiment to be considered a research design model [27].

Several works, whose main goal is to optimize manufacturing process, can be found in the literature, such as [28–31]. The authors commonly apply techniques such as factor analysis, normal boundary intersection (NBI), and response surface methodology (RSM) for multiobjective optimization.

A study to understand how the metal inert gas (MIG) process parameters affect the geometric characteristics of a 6063-T5 aluminum alloy weld bead is developed in [28]. The experimental design consisted of three variables (power of the source, welding speed, and separation between the edges of the base metal), with three levels each, and then nine experiments were performed according to an orthogonal Taguchi array. The study identified the optimal values for the input parameters in order to maximize the penetration and minimize the remaining responses, i.e., bead height, root width, overthickness, perimeter, and area of filler material.

The interactions between the variables of the continuous drive friction welding (CDFW) process were analyzed at the junction of AA6063 aluminum tubes in [29]. The authors applied a full factorial design with three levels for each input variable (rotation, friction pressure, and friction time on the final dimensions of the flash and length of the welded piece). Twenty-seven experiments were run, and the lowest pressure value produced the specimens with the lowest reduction values in length and uniform flashes.

In [30], a numerical study of time-temperature-property curves was developed considering the 6063-T5 aluminum alloy plates by using the MIG technique. A Taguchi array was used with two levels for the two parameters, source power and welding speed, allowing the optimization of the intersection area between the cooling curve and the cooling time between 400 and 300 °C.

A new methodology was proposed in [31] to optimize a multivariate dry end milling process of the AISI 1045 steel. The considered parameters were the feed per tooth, axial depth of cut, cutting speed, and radial depth of cut. It was possible to encounter the input combination which led to maximum material removal rate and minimum surface roughness, through techniques such as normal boundary intersection (NBI) and multivariate mean square error (MMSE).

Then, it could be observed that some published papers apply a design of experiments and multivariate techniques

and even hybrid approaches such as NBI-MMSE. Nevertheless, in multivariate problems, where two or more responses are being simultaneously optimized, some additional caution may be taken in order to consider the possible correlation between the output variables, since feasible values for one variable might not occur simultaneously with feasible values for another output variable because of the correlation structure.

Thus, the new approach of this study is to use Bonferroni’s multivariate intervals to establish the limits that the responses may assume in the optimization problem. Elliptical constraints will also be used considering the variance and covariance structure of the responses. The responses will be modeled, initially, using the method of ordinary least squares (OLS), and then, the resulting quadratic residues will be modeled using Poisson regression. In this sense, the weighted least squares algorithm could be applied to the original responses, increasing the model adjustments.

3 Background and literature review

3.1 Response surface methodology

Response surface methodology (RSM) is a design of experiment (DOE) technique to model and analyze complex problems in which an optimal response is sought for a variable of interest influenced by so many other process variables [32].

Since this methodology is practical, economical, and easy to implement [33], it is widely applied in the industrial sector, mainly in scenarios where the quality of the product or process, or even the performance measures, is influenced by many input variables [34] and because this relationship is typically unknown [35].

Costa et al. [31] applied the multivariate optimization using the RSM to a dry milling process of AISI 1045, considered more sustainable than the conventional milling process, since it does not use cutting fluids. Lu and Xu [36] used this methodology to find the best conditions for a new non-leaching gold recovery strategy from discarded memory cards. Nasiri and Arsalani [37] used the RSM to assess the influence of experimental factors, such as initial dye concentration, contact time, initial pH, and adsorbent dosage on the efficiency of removing violet crystals, to subsequently find the optimum condition of these variables that would maximize the objective function. However, countless applications available in the literature prove that, although widely used in industries, its application is highly diversified.

RSM depends on the elaboration of an experimental design to guide, in a more assertive way, through a reduced number of experiments, the obtaining of real output data process, in order to make possible the definition of an analytical model that approximates the accurate relationship between the

responses of interest and the decision variables, in some region of interest [34].

According to [38], the second-order polynomial presented in Eq. (1) satisfactorily represents the problems for the response surface. In the equation, Y represents the answer of interest to the problem, β represents the coefficients to be estimated, k indicates the number of independent variables, x represents the parameters, and, finally, ε represents the error associated with the responses. The coefficients are estimated using the widely used regression method called ordinary least squares (OLS) [39–41].

$$Y = \beta_0 + \sum_{i=1}^k \beta_i x_i + \sum_{i=1}^k \beta_{ii} x_i^2 + \sum_{i < j} \beta_{ij} x_i x_j + \varepsilon \tag{1}$$

The quadratic design named central composite design (CCD) for k factors is extensively used to estimate second-order response surfaces [31]. It consists of a resolution V fractional factorial arrangement or a 2^k factorial design, added with n_c central points and 2^k axial points [34]. Its representation can be seen in the CCD (Fig. 1).

Some analysis must be carried out to guarantee the adequacy of the models to the process in question. High values of coefficients such as R^2 and R^2_{adj} that are obtained through the ANOVA technique, for example, indicate a good level of fit for the model [34]. Montgomery [32] also states that an analysis of normality of residues can ratify the information obtained in ANOVA.

Whether the models have adequate fit and residuals, this becomes sufficient for the subsequent application of a multiobjective optimization algorithm to define the optimum point, or the set of optimal points, that will determine the optimal operating conditions for the process.

3.2 Multiobjective optimization

Multiobjective optimization is an approach used to deal with scenarios where more than one characteristic of the process needs to be optimized simultaneously and can be generically described by Eq. (2) [42].

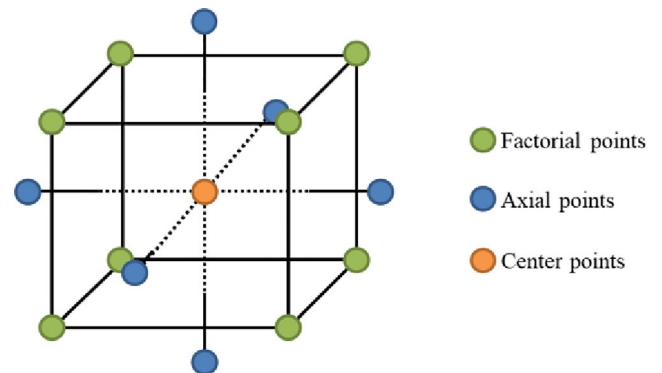


Fig. 1 CCD for 3 factors representation

$$\min_{x \in C} F(x) = \begin{bmatrix} f_1(x) \\ f_2(x) \\ \vdots \\ f_n(x) \end{bmatrix}, n > 2, \dots(\text{MOP}) \tag{2}$$

$$C = \{x : h(x) = 0, g(x) \leq 0, a \leq x \leq b\}$$

where a and b are the limits that restrict the solution space and $h(x)$ and $g(x)$ characterize the equality and inequality constraints, respectively.

According to the principle established by Pareto, a multiobjective problem does not offer a single optimal solution, due to the existing trade-off relationship between the characteristics of the system, but a set of solutions called Pareto optimal. That is, there is no solution x^* such that all of the objective functions $f_i(x)$ are minimized at the same time [42].

To deal with this issue, methods such as the normal boundary intersection (NBI) generate a border containing feasible solutions, called Pareto optimal, making the problem analysis within the industry more practical and visual [43].

The main contribution of the NBI method is the construction of a balanced Pareto boundary with optimal equidistant solutions, which exceeds the performance of the least squares method. The general formulation for a problem to be solved by the NBI can be written as a restricted nonlinear programming and can be seen in Eq. (3) [42].

$$\begin{aligned} \max_{x,t} t & \tag{3} \\ \text{s.t. } \bar{\Phi}\beta + t\hat{n} = \bar{F}(x) \\ h_i(x) &= 0 \\ g_j(x) &\leq 0 \\ a \leq x &\leq b \end{aligned}$$

where in the first constraint $\bar{\Phi}\beta + t\hat{n} = \bar{F}(x)$, $\bar{\Phi}$ represents the normalized *payoff* matrix, β indicates the vector of weights for each, t corresponds to a scalar that is perpendicular to the utopia line, and $\bar{F}(x)$ is the vector of dimensioned objective functions [21].

For the *payoff* matrix composition Φ , the functions must be individually optimized so that the i th line of the matrix presents, in its position Φ_{ii} , the optimal value of $f_i(x^*)$. The remaining positions of this same line show the values of the other functions evaluated in the i th optimal point x_i^* . This ensures that the diagonal of the matrix contains all the optimal values of the individual functions involved in the problem [41–44].

The $\bar{\Phi}$ matrix, in turn, is obtained from the normalization of each of the positions of the original payoff matrix. The utopia vector contains the individual optimal of all functions, such that $f^U = [f_1^*(x_1^*), \dots, f_i^*(x_i^*), \dots, f_m^*(x_m^*)]^T$. This generally does not characterize a viable scenario for the process [21].

The nadir vector contains the worst possible value for all functions, among the values found in Φ , so that $f^N = [f_1^N, \dots, f_i^N, \dots, f_m^N]^T$. Thus, the normalized matrix $\bar{\Phi}$ will be obtained from Eq. (4) [45].

$$\bar{f}_i(x) = \frac{f_i(x) - f_i^U}{f_i^N - f_i^U} \tag{4}$$

In this way, it is possible to observe the general composition of the matrices Φ and $\bar{\Phi}$ through Eqs. 5 and 6.

$$\Phi = \begin{bmatrix} f_1^*(x_1^*) & \dots & f_1^*(x_i^*) & \dots & f_1^*(x_m^*) \\ \vdots & \ddots & \vdots & \ddots & \vdots \\ f_i^*(x_1^*) & \dots & f_i^*(x_i^*) & \dots & f_i^*(x_m^*) \\ \vdots & \ddots & \vdots & \ddots & \vdots \\ f_m^*(x_1^*) & \dots & f_m^*(x_i^*) & \dots & f_m^*(x_m^*) \end{bmatrix} \tag{5}$$

$$\bar{\Phi} = \begin{bmatrix} \bar{f}_1^*(x_1^*) & \dots & \bar{f}_1^*(x_i^*) & \dots & \bar{f}_1^*(x_m^*) \\ \vdots & \ddots & \vdots & \ddots & \vdots \\ \bar{f}_i^*(x_1^*) & \dots & \bar{f}_i^*(x_i^*) & \dots & \bar{f}_i^*(x_m^*) \\ \vdots & \ddots & \vdots & \ddots & \vdots \\ \bar{f}_m^*(x_1^*) & \dots & \bar{f}_m^*(x_i^*) & \dots & \bar{f}_m^*(x_m^*) \end{bmatrix} \tag{6}$$

Therefore, for bi-objective scenarios, the classic NBI formulation represented by Eqs. (3) and (4) and matrix (6) can be rewritten according to Eq. (7). For the Pareto frontier construction, this problem is solved iteratively by applying different weights [45].

$$\begin{aligned} \min_x F(x) &= \bar{f}_1(x) & \tag{7} \\ \text{s.t. } \bar{f}_1(x) - \bar{f}_2(x) + 2\beta_1 - 1 &= 0 \\ x &\in \Omega \\ g_j(x) &\leq 0 \\ h_{j+1}(x) &= 0 \end{aligned}$$

3.3 Poisson regression

When the response variable of interest is not normally distributed, and it represents a count of some relatively rare event, Poisson regression is a technique that is possible to be applied. In these cases, a probability model can be obtained as shown in Eq. (8) where μ_i and y_i represent the mean and the i th observation, respectively [46].

$$f(y_i) = \frac{e^{-\mu_i} \mu_i^{y_i}}{y_i!} \tag{8}$$

According to the same author, the Poisson model is written in terms of the mean response. It is necessary to suppose that there is a function g , which establishes the relationship

between the mean and a linear predictor as in Eq. (9). The function g is called link function.

$$g(\mu_i) = \eta_i = \beta_0 + \beta_1 x_1 + \dots + \beta_k x_k = \mathbf{x}_i^T \boldsymbol{\beta} \tag{9}$$

Thus, Eq. (10) will give the relationship between the mean and the linear predictor.

$$\mu_i = g^{-1}(\eta_i) = g^{-1}(\mathbf{x}_i^T \boldsymbol{\beta}) \tag{10}$$

A function commonly used for the Poisson distribution is the log link, that is, $\mu_i = e^{\mathbf{x}_i^T \boldsymbol{\beta}}$. This is very useful in Poisson regression problems because it provides only nonnegative predictions for the response variable. Besides, the maximum likelihood method is used to estimate the unknown parameters. Considering a sample of n observations, where y is the response of interest and x represents the predictors, then the likelihood function can be written as shown in Eq. (11) [46].

$$\mathcal{L}(\boldsymbol{\beta}; \mathbf{y}) = \prod_{i=1}^n \frac{e^{-\mu_i} \mu_i^{y_i}}{y_i!} = \frac{\prod_{i=1}^n \mu_i \exp\left(-\sum_{i=1}^n \mu_i\right)}{\prod_{i=1}^n y_i!} \tag{11}$$

After selecting the link function, the log-likelihood shown in Eq. (12) is maximized.

$$\ln \mathcal{L}(\boldsymbol{\beta}; \mathbf{y}) = \sum_{i=1}^n y_i \ln(\mu_i) - \sum_{i=1}^n \mu_i - \sum_{i=1}^n \ln(y_i!) \tag{12}$$

Once the estimates of the parameters are encountered, the prediction equation will be as in Eq. (13) if the log link function was chosen.

$$\hat{y}_i = g^{-1}(\mathbf{x}_i^T \mathbf{b}) = \exp(\mathbf{x}_i^T \mathbf{b}) \tag{13}$$

3.4 Simultaneous confidence intervals

In multivariate problems, constructing simultaneous confidence intervals is more sophisticated than simply analyzing individual intervals, since the first considers the correlation structure of the analyzed responses.

Let \mathbf{X} have an $N_p(\boldsymbol{\mu}, \boldsymbol{\Sigma})$ distribution, and \mathbf{Z} is the linear combination $\mathbf{a}^T \mathbf{X}$, where \mathbf{a}^T is a constant vector. Then, \mathbf{Z} has an $N_p(\mathbf{a}^T \boldsymbol{\mu}, \mathbf{a}^T \boldsymbol{\Sigma} \mathbf{a})$ distribution. Regarding an available random sample of \mathbf{X} , it is possible to replace $\boldsymbol{\mu}$ and $\boldsymbol{\Sigma}$ with $\bar{\mathbf{x}}$ and \mathbf{S} , respectively. For a given \mathbf{a} , the $100(1-\alpha)\%$ confidence interval is based on Eq. (14) [47].

$$t = \frac{\bar{z} - \mu_z}{s_z/n} = \frac{\sqrt{n}(\mathbf{a}^T \bar{\mathbf{x}} - \mathbf{a}^T \boldsymbol{\mu})}{\sqrt{\mathbf{a}^T \mathbf{S} \mathbf{a}}} \tag{14}$$

which leads to Eq. (15).

$$\mathbf{a}^T \bar{\mathbf{x}} - t_{n-1}(\alpha/2) \frac{\sqrt{\mathbf{a}^T \mathbf{S} \mathbf{a}}}{\sqrt{n}} \leq \mathbf{a}^T \boldsymbol{\mu} \leq \mathbf{a}^T \bar{\mathbf{x}} + t_{n-1}(\alpha/2) \frac{\sqrt{\mathbf{a}^T \mathbf{S} \mathbf{a}}}{\sqrt{n}} \tag{15}$$

Considering a determined dataset and a vector \mathbf{a} , the confidence interval is the set of values for $\mathbf{a}^T \boldsymbol{\mu}$ that satisfies Eq. (16).

$$t^2 = \frac{n(\mathbf{a}^T \bar{\mathbf{x}} - \mathbf{a}^T \boldsymbol{\mu})^2}{\mathbf{a}^T \mathbf{S} \mathbf{a}} \leq t_{n-1}^2(\alpha/2) \tag{16}$$

Thus, according to the Cauchy-Schwarz inequality, maximizing t^2 in terms of vector \mathbf{a} leads to Eq. (17), where T^2 is the Hotelling statistic and c^2 is a constant larger than t^2 .

$$\max_{\mathbf{a}} \frac{n(\mathbf{a}^T (\bar{\mathbf{x}} - \boldsymbol{\mu}))^2}{\mathbf{a}^T \mathbf{S} \mathbf{a}} = n(\bar{\mathbf{x}} - \boldsymbol{\mu})^T \mathbf{S}^{-1} (\bar{\mathbf{x}} - \boldsymbol{\mu}) = T^2 \leq c^2 \tag{17}$$

When $c^2 = p(n-1)F_{p, n-p}(\alpha)/(n-p)$, it is possible to encounter the intervals that contain $\mathbf{a}^T \boldsymbol{\mu}$ for all \mathbf{a} with probability $1 - \alpha = P[T^2 \leq c^2]$ as shown in Eq. (18).

$$\begin{aligned} \mathbf{a}^T \bar{\mathbf{X}} - \sqrt{\frac{p(n-1)}{n(n-p)} F_{p, n-p}(\alpha)} \mathbf{a}^T \mathbf{S} \mathbf{a} \leq \mu \leq \mathbf{a}^T \bar{\mathbf{X}} \\ + \sqrt{\frac{p(n-1)}{n(n-p)} F_{p, n-p}(\alpha)} \mathbf{a}^T \mathbf{S} \mathbf{a} \end{aligned} \tag{18}$$

In order to find the confidence interval for each mean, simply assume $\mathbf{a}^T = [1, 0, \dots, 0]$, $\mathbf{a}^T = [0, 1, \dots, 0]$, and so on. Then, Eq. (19) can replace Eq. (18).

$$\begin{aligned} \bar{x}_p - \sqrt{\frac{s_{pp}(n-1)p}{n(n-p)} F_{p, n-p}(\alpha)} \leq \mu \leq \bar{x}_p \\ + \sqrt{\frac{s_{pp}(n-1)p}{n(n-p)} F_{p, n-p}(\alpha)} \end{aligned} \tag{19}$$

An alternative method for multiple comparisons that can be applied in multivariate problems when the number of component means is small is the Bonferroni method. Applying this method, the intervals are shorter and more precise than previously presented. Equation (20) shows how to calculate them [47].

$$\bar{x}_p - t_{n-1} \left(\frac{\alpha}{2p} \right) \sqrt{\frac{s_{pp}}{n}} \leq \mu_p \leq \bar{x}_p + t_{n-1} \left(\frac{\alpha}{2p} \right) \sqrt{\frac{s_{pp}}{n}} \tag{20}$$

Figure 2 depicts how the Bonferroni intervals are shorter than the simultaneous T^2 intervals (shadows). These ellipsoids were constructed using the cladding data presented in this paper.

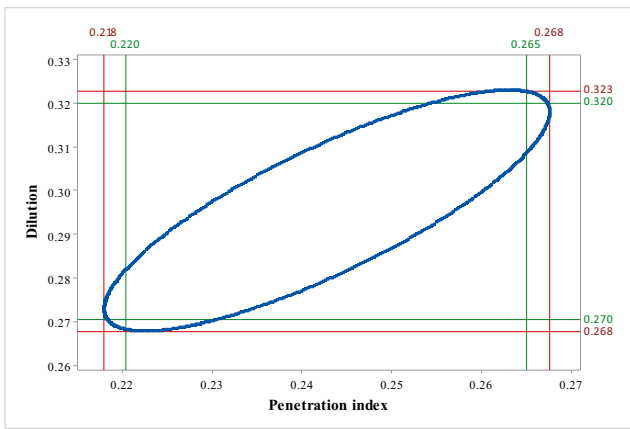


Fig. 2 Simultaneous Hotelling and Bonferroni intervals

The ellipsoid shown in Fig. 3 and all the other confidence ellipsoids for the mean of the variables presented in this paper were constructed according to Eq. (21) found in [21], where μ_{y_i} indicates the mean of the variables; p and n are the number of variables and the number of data, respectively; F is the statistic associated with α significance level; λ_i represents the eigenvalues; e_{ij} represents the elements of the matrix composed of the eigenvectors; and θ is an angle varying from 0 to 2π .

$$\begin{bmatrix} \mu_{y_1} \\ \mu_{y_2} \end{bmatrix} + \sqrt{\frac{p(n-1)}{n(n-p)} F_{(p,n-p)}(\alpha)} \times \begin{bmatrix} \sqrt{\lambda_1} & 0 \\ 0 & \sqrt{\lambda_2} \end{bmatrix} \times \begin{bmatrix} e_{11} & e_{12} \\ e_{21} & e_{22} \end{bmatrix} \times \begin{bmatrix} \cos\theta \\ \sin\theta \end{bmatrix} \quad (21)$$

On the other hand, the ellipsoids for the data are created following Eq. (22).

$$\begin{bmatrix} \mu_{y_1} \\ \mu_{y_2} \end{bmatrix} + c \times \begin{bmatrix} e_{11} & e_{12} \\ e_{21} & e_{22} \end{bmatrix} \times \begin{bmatrix} \sqrt{\lambda_1} & 0 \\ 0 & \sqrt{\lambda_2} \end{bmatrix} \times \begin{bmatrix} \cos\theta \\ \sin\theta \end{bmatrix} \quad (22)$$

3.5 Factor analysis

Grouping variables highly correlated, resulting in high correlation values within the formed groups and small correlation

values between different groups, this is the argument that motivates the factor analysis (FA). The main purpose of this technique is to express the covariance relationships among distinct variables in terms of unobservable variables called factors [47]. Factor analysis can be considered an extension of the principal component analysis (PCA). Nevertheless, a great difference is that in PCA the principal components (PCs) are written in terms of the standardized variables, whereas in FA the variables are written in terms of the uncorrelated factors.

According to [48], in the factor analysis model, a problem with m observed variables may lead to unobserved scores for the p factors with $m > p$. That is, the main function of the different factor analysis techniques is to reduce a large number of variables observed in a fewer number of factors [49], and define the factor as the linear combination of the original (statistics) variables.

Let \mathbf{X} be an observable vector with p components, mean vector $\boldsymbol{\mu}$, and covariance matrix $\boldsymbol{\Sigma}$. Hence, \mathbf{X} will be linearly dependent upon the uncorrelated variables F_1, F_2, \dots, F_m (common factors) and $\varepsilon_1, \varepsilon_2, \dots, \varepsilon_p$ (specific factors). Equation (23) represents the factor analysis model according to [47], where l_{ij} represents the loadings, explained later in this section.

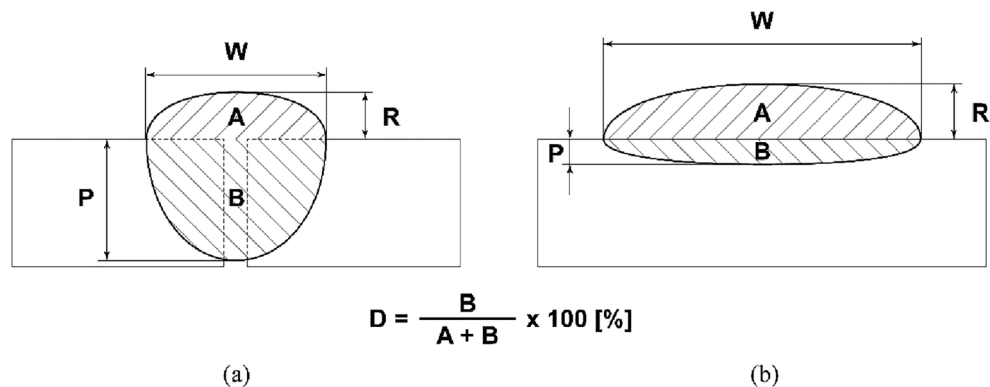
$$\begin{aligned} X_1 - \mu_1 &= l_{11}F_1 + l_{12}F_2 + \dots + l_{1m}F_m + \varepsilon_1 \\ X_2 - \mu_2 &= l_{21}F_1 + l_{22}F_2 + \dots + l_{2m}F_m + \varepsilon_2 \\ &\vdots \\ X_p - \mu_p &= l_{p1}F_1 + l_{p2}F_2 + \dots + l_{pm}F_m + \varepsilon_p \end{aligned} \quad (23)$$

Consider that \mathbf{F} and $\boldsymbol{\varepsilon}$ are the matrices containing the common and specific factors, respectively. Also, assuming that $E(\mathbf{F}) = 0$; $\text{Cov}(\mathbf{F}) = E[\mathbf{F}'\mathbf{F}] = \mathbf{I}$; $E(\boldsymbol{\varepsilon}) = 0$, $\text{Cov}(\boldsymbol{\varepsilon}) = E[\boldsymbol{\varepsilon}\boldsymbol{\varepsilon}'] = \boldsymbol{\Psi}$, which is a diagonal matrix whose elements in the main diagonal are $\psi_1, \psi_2, \dots, \psi_p$, and finally that $\text{Cov}(\boldsymbol{\varepsilon}, \mathbf{F}) = E(\boldsymbol{\varepsilon}\mathbf{F}') = 0$, hence the orthogonal model can be estimated as shown in Eq. (24) in matrix notation [47].

$$\mathbf{X}_{(p \times 1)} = \boldsymbol{\mu}_{(p \times 1)} + \mathbf{L}_{(p \times m)}\mathbf{F}_{(m \times 1)} + \boldsymbol{\varepsilon}_{(p \times 1)} \quad (24)$$

where μ_i and ε_i represent the mean and the specific factor of the i th variable, respectively. F_j is the j th common factor and l_{ij}

Fig. 3 Weld bead geometry (a), union of the welded joint (conventional applications) (b) [23]



is the loading of the i th variable on the j th factor. Thus, this model implies that the covariance structure can be written as shown in Eq. (25).

$$\begin{aligned} \Sigma &= Cov(X) = E(X-\mu)(X-\mu)^T \\ \Sigma &= LE(FF^T)L^T + E(\varepsilon\varepsilon^T)L^T + LE(F\varepsilon^T) + E(\varepsilon\varepsilon^T) \\ \Sigma &= LL^T + \Psi \end{aligned} \quad (25)$$

In this sense, from Eq. (2), the variance and the covariance of the original variables can be written as in Eq. (26).

$$\begin{aligned} Var(X_i) &= \underbrace{l_{i1}^2 + \dots + l_{im}^2}_{\text{communality}} + \underbrace{\psi_i}_{\text{specific variance}} \\ Cov(X_i, X_k) &= l_{i1}l_{k1} + \dots + l_{im}l_{km} \end{aligned} \quad (26)$$

It can also be drawn that $Cov(\mathbf{X}, \mathbf{F}) = E(\mathbf{X}-\mu)\mathbf{F}^T = LE(\mathbf{F}\mathbf{F}^T) + E(\varepsilon\mathbf{F}^T) = \mathbf{L}$. Thus, it is possible to state that the loading (l_{ij}) represents the covariance between the observations of the i th variable and the j th factor.

The principal component estimation method is commonly used in factor analysis. Usually p variables are written as linear combinations of m factors with $m < p$. This results in the following approximation for the variance-covariance matrix as in Eq. (27), which is known as the principal component solution when applied to sample variance-covariance matrix \mathbf{S} or to the sample correlation matrix \mathbf{R} [47].

$$\Sigma = \left[\sqrt{\lambda_1}e_1 \mid \sqrt{\lambda_2}e_2 \mid \dots \mid \sqrt{\lambda_m}e_m \right] \begin{bmatrix} \psi_1 & 0 & \dots & 0 \\ 0 & \psi_2 & \dots & 0 \\ \vdots & \vdots & \ddots & \vdots \\ 0 & 0 & \dots & \psi_m \end{bmatrix} \quad (27)$$

3.6 Factor mean square error

It is common to represent more than one response variable by just one factor using factor analysis. However, it might happen that variables represented by the same factor are conflicting in terms of optimization direction, which means that the same factor may explain a variable to be maximized and a variable to be minimized. Paiva et al. [50] proposed an approach to deal with this type of problem called multivariate mean square error (MMSE) using principal component analysis.

In the present paper, the factor analysis is applied, and it proposed the factor mean square error (FMSE), which is based on MMSE previously mentioned, but considering factor analysis. Equation (28) is used to calculate the FMSE, where $\hat{F}_i(\mathbf{x})$ represents the fitted value for the i th factor, T_i is the target calculated for this factor, and λ_i is the variance associated with the factor.

$$FMSE_i = \left[\hat{F}_i(\mathbf{x}) - T_i \right]^2 + \lambda_i \quad (28)$$

In order to calculate target of each factor, Eq. (29) must be used.

$$T_i = \mathbf{L}_i\mathbf{Z} \quad (29)$$

\mathbf{L}_i is the vector of loadings related to the i th factor, and \mathbf{Z} is a vector of standardized values. Each value of \mathbf{Z} is calculated as shown in Eq. (30), where μ_j , ζ_j , and σ_j are the mean value, the individual target, and the standard deviation of the j th variable, respectively.

$$Z = \left(\frac{\mu_j - \zeta_j}{\sigma_j} \right) \quad (30)$$

4 Methodology

The present paper introduces a new approach to solve multivariate problems. The methodology was applied in a cladding process of ABNT 1020 carbon steel plate using austenitic ABNT 316L stainless steel cored wire performed in [22]. The authors ran 31 designed experiments from a central composite design following the stages of the response surface methodology presented in [32]. The input parameters and their respective levels are presented in Table 1.

The investigated responses in the present paper are the dilution (D), yield (Y), penetration index (PI), and convexity index (CI). D represents the ratio between the penetration area and the total area (penetration and reinforcement). Y is the ration between the deposition rate and the fusion rate. The

Table 1 Parameters considered in the cladding process and their respective levels

Parameters	Abbreviation	Levels				
		-2	-1	0	1	2
Wire feed rate (m/min)	<i>WF</i>	5.5	7.0	8.5	10.0	11.5
Arc voltage (V)	<i>V</i>	24.5	27.0	29.5	32.0	34.5
Welding speed (cm/min)	<i>WS</i>	20.0	30.0	40.0	50.0	60.0
Contact tip to the workpiece distance (mm)	<i>CT</i>	10.0	15.0	20.0	25.0	30.0

two considered indexes are calculated considering the geometric characteristics of the weld bead. *PI* is calculated dividing the penetration by the thickness of the sheet, whereas *CI* is calculated dividing the reinforcement by the width.

In order to illustrate the concepts previously mentioned, Fig. 3 depicts the geometry of a weld bead, where *P* represents the penetration, *W* is the width, *R* is the reinforcement, and *A* and *B* are the reinforcement and penetration areas, respectively.

The methodology itself is based on incorporating multivariate intervals and elliptical constraints to the multiobjective optimization problem. The Poisson regression technique is also applied in order to model the squared residuals from the OLS models for the factors and the original variables. Figure 4 depicts the complete methodology used in this paper, and a short explanation about its stages can be found in this section. It is important to highlight that this methodology is only applicable when dealing with multivariate data, i.e., correlated data.

A. Evaluate the correlation

Initially, the correlation structure of the dataset must be evaluated. Frequently many correlated variables are treated

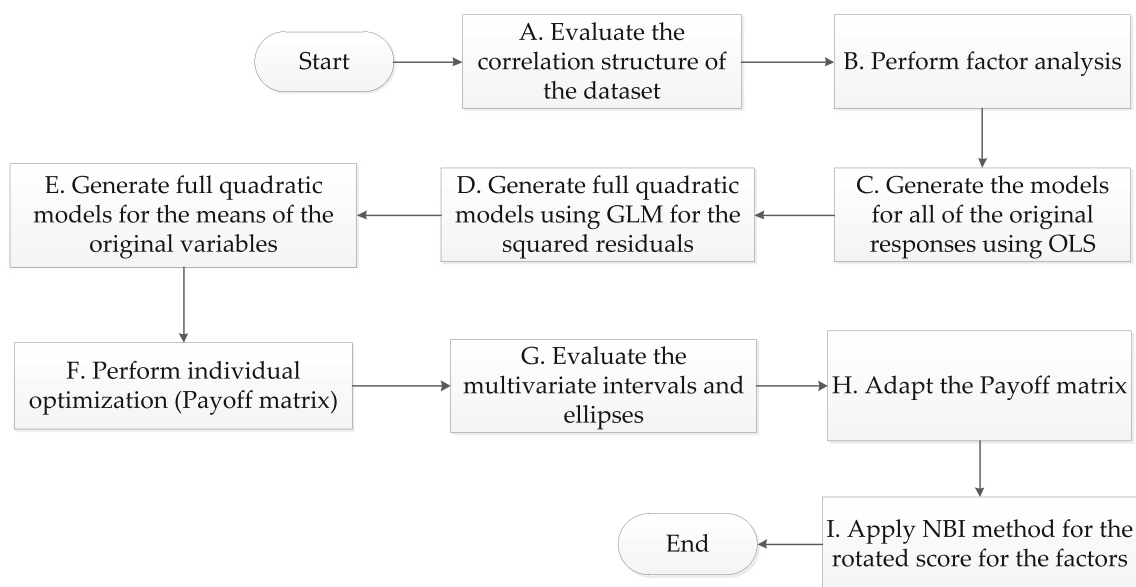
as uncorrelated, and it may lead to erroneous conclusions about the problem. Thus, it is necessary to calculate the correlation between all pairs of variables as well as the *p* values associated. Usually, Pearson correlation is applied.

B. Factor analysis

Considering correlated variables, a multivariate technique such as factor analysis can be applied in order to replace the original variables by unobservable variables, i.e., rotated factor scores. The correlation between the factors and the original variables determines the loading values, which indicate how much a factor is able to explain a certain variable. However, the correlation between each pair of factors is always zero.

C. OLS models

The investigated responses are modeled using traditional algorithms such as ordinary least squares (OLS), and the residuals of the models must be stored.

**Fig. 4** Methodology for multiobjective optimization considering multivariate constraints

D. Poisson models for the residuals

Next, the squared residuals are modeled through Poisson regression according to Eq. (13). The fitted values for the squared residuals are also stored.

E. Poisson models for original variables

The weight $W = 1/\hat{e}_i^2$ is calculated, where e_i^2 represents the residuals stored in the phase **D**. The full quadratic models for the original variables are now obtained through weighted Poisson regression.

F. Individual optimization

Once these models are estimated, it is possible to obtain the individual optimal values for the original variables. It is important to mention that *DR*, *PI*, and *RI* must be minimized, whereas *Y* is the only response to be maximized. With the values generated by the optimization, the payoff matrix is constructed according to Eq. (5).

G. Multivariate analysis

In this phase, Bonferroni’s simultaneous intervals are calculated according to Eq. (20). The confidence ellipsoids for the mean data are also calculated as shown in Eq. (21). It is important to consider them because the data are correlated, which means that the variables vary together, and therefore, a value for a certain variable may never occur simultaneously with a value for another correlated variable even though both values are feasible.

H. Payoff adaptation

After the multivariate analysis, it is necessary to adapt the payoff matrix calculated in **H** considering the multivariate constraints from the previous step.

I. Multiobjective optimization

$$\begin{aligned}
 F_1 &= 0.3438 + 0.0639 \times WF + 0.5141 \times V + 0.4070 \times WS - 0.7481 \times CT \\
 &- 0.1828 \times V^2 > -0.2613 \times WS^2 + 0.1979 \times WF \times V - 0.1872 \times WF \times CT \\
 R^2 &= 92.60\% \\
 R_{adj}^2 &= 89.91\%
 \end{aligned}
 \tag{31}$$

$$\begin{aligned}
 F_2 &= -0.817 + 0.2975 \times WF + 0.2005 \times V - 0.5628 \times WS - 0.4625 \times CT + \\
 &2200 \times WF^2 + 0.3339 \times V^2 + 0.1926 \times WS^2 + 0.3089 \times CT^2 + 0.3120 \times WF \times CT \\
 R^2 &= 87.90\% \\
 R_{adj}^2 &= 80.90\%
 \end{aligned}
 \tag{32}$$

The factor mean squared error (FMSE_{*i*}) function is calculated for the *i* factors encountered in phase **B** using Eq. (28). Finally, the NBI method can be applied in order to calculate the Pareto frontier and evaluate the results.

5 Results

This section presents the results obtained in each phase of the previously explained methodology.

A. Evaluate the correlation

The data used in this paper was originated from the cladding process previously presented in [22]. The authors performed 31 designed experiments as shown in Table 2. The correlation structure in the data can be observed in Table 3, where a *p* value less than 0.05 represents a significant correlation value.

B. Factor analysis

The factor analysis was performed using the Minitab software considering the correlation matrix, the rotation varimax, and the principal components as the extraction method. Two factors were able to explain 85.4% of the variability in the data. Table 4 shows the rotated factor scores for each run of the CCD, which means that the data are now represented by two uncorrelated factors.

The factors are highly correlated with the variables that they represent as can be viewed in Table 5 that shows the loading for each factor, the communalities, the variance, and the percentage of explained variance.

C. OLS models

Both the factors and the original variables can be modeled using ordinary least squares algorithm. The models for each response and the values for *R*² and *R*²_{adjusted} can be viewed in Eqs. (31)–(36).

Table 2 Designed experiments and values for the investigated responses

Run	WF	V	WS	CT	D	Y	CI	PI
1	7	27	30	15	0.2644	0.8974	0.2349	0.2165
2	10	27	30	15	0.2582	0.8971	0.2398	0.2616
3	7	32	30	15	0.3149	0.8914	0.1966	0.2660
4	10	32	30	15	0.3125	0.8947	0.1846	0.3113
5	7	27	50	15	0.3622	0.9158	0.2350	0.2593
6	10	27	50	15	0.3369	0.9070	0.2677	0.3049
7	7	32	50	15	0.3712	0.8743	0.2118	0.2422
8	10	32	50	15	0.4108	0.8836	0.2107	0.3434
9	7	27	30	25	0.2246	0.9049	0.2780	0.1969
10	10	27	30	25	0.1832	0.8947	0.3145	0.1574
11	7	32	30	25	0.2371	0.9060	0.2528	0.2081
12	10	32	30	25	0.2196	0.8981	0.2384	0.1733
13	7	27	50	25	0.2496	0.9403	0.3196	0.1750
14	10	27	50	25	0.2331	0.9017	0.3243	0.1930
15	7	32	50	25	0.2877	0.9352	0.2788	0.2157
16	10	32	50	25	0.3019	0.9174	0.2397	0.2578
17	5.5	29.5	40	20	0.3156	0.9262	0.2434	0.2177
18	11.5	29.5	40	20	0.3095	0.8952	0.2502	0.3369
19	8.5	24.5	40	20	0.2284	0.9041	0.3211	0.1897
20	8.5	34.5	40	20	0.3558	0.9004	0.2103	0.2936
21	8.5	29.5	20	20	0.1858	0.9027	0.2313	0.1492
22	8.5	29.5	60	20	0.3578	0.9308	0.2652	0.2256
23	8.5	29.5	40	10	0.4044	0.8815	0.2225	0.3431
24	8.5	29.5	40	30	0.2416	0.9205	0.3136	0.2020
25	8.5	29.5	40	20	0.3105	0.9304	0.2399	0.2690
26	8.5	29.5	40	20	0.3167	0.9191	0.2373	0.2713
27	8.5	29.5	40	20	0.3088	0.9251	0.2471	0.2556
28	8.5	29.5	40	20	0.3283	0.9198	0.2351	0.2837
29	8.5	29.5	40	20	0.2999	0.9215	0.2464	0.2339
30	8.5	29.5	40	20	0.3109	0.9240	0.2467	0.2346
31	8.5	29.5	40	20	0.3102	0.9258	0.2419	0.2369

Table 4 Rotated factor scores

Run	WF	V	WS	CT	F1	F2
1	7	27	30	15	-0.4531	0.9042
2	10	27	30	15	-0.1923	0.8868
3	7	32	30	15	0.5620	1.2391
4	10	32	30	15	1.0148	1.1115
5	7	27	50	15	0.8539	-0.5561
6	10	27	50	15	0.6755	-0.2029
7	7	32	50	15	0.5524	1.8591
8	10	32	50	15	1.7601	1.1175
9	7	27	30	25	-1.1691	0.3931
10	10	27	30	25	-2.1802	0.9238
11	7	32	30	25	-0.7856	0.4393
12	10	32	30	25	-1.1706	1.0636
13	7	27	50	25	-1.0923	-1.9190
14	10	27	50	25	-1.5015	0.2353
15	7	32	50	25	-0.2185	-1.5622
16	10	32	50	25	0.3338	-0.4149
17	5.5	29.5	40	20	0.1927	-0.9542
18	11.5	29.5	40	20	0.7142	0.6540
19	8.5	24.5	40	20	-1.5190	0.1492
20	8.5	34.5	40	20	1.0960	0.4613
21	8.5	29.5	20	20	-1.5335	1.0158
22	8.5	29.5	60	20	0.4820	-1.5354
23	8.5	29.5	40	10	1.5992	1.1801
24	8.5	29.5	40	30	-1.0994	-0.7695
25	8.5	29.5	40	20	0.6179	-1.1780
26	8.5	29.5	40	20	0.5933	-0.5640
27	8.5	29.5	40	20	0.3935	-0.9132
28	8.5	29.5	40	20	0.8063	-0.6474
29	8.5	29.5	40	20	0.1235	-0.6605
30	8.5	29.5	40	20	0.2395	-0.8451
31	8.5	29.5	40	20	0.3044	-0.9114

Table 3 Correlation structure

	D	Y	CI
Y	-0.1070		
	0.5650		
CI	-0.5840	0.3690	
	0.0010	0.0410	
PI	0.8180	-0.2900	-0.6010
	0.0000	0.1140	0.0000

Pearson correlation (above) and *p* value (below)

Table 5 Factor analysis summary

Variable	Factor 1	Factor 2	Communality
D	0.9475	-0.0403	0.899
PI	0.9099	0.1714	0.857
CI	-0.7295	-0.4110	0.701
Y	-0.1029	-0.9735	0.958
Variance	2.2684	1.1475	3.4159
% Var	0.567	0.287	0.854

$$\begin{aligned}
 D &= 0.31034 - 0.00282 \times WF + 0.02493 \times V + 0.03679 \times Vs - 0.04251 \times N \\
 &\quad - 0.00723 \times T^2 - 0.01229 \times Vs^2 + 0.00769 \times WF \times V - 0.00771 \times Ws \times CT \\
 R^2 &= 95.55\% \\
 R^2_{adj} &= 93.93\%
 \end{aligned}
 \tag{33}$$

$$\begin{aligned}
 Y &= 0.92367 - 0.00554 \times WF - 0.00274 \times V + 0.00613 \times WS + 0.00895 \times CT \\
 &\quad - 0.00390 \times WF^2 - 0.00602 \times V^2 - 0.00238 \times WS^2 - 0.00632 \times CT^2 \\
 &\quad - 0.00487 \times WF \times CT - 0.00315 \times V \times WS + 0.00553 \times V \times CT \\
 R^2 &= 89.12\% \\
 R^2_{adj} &= 81.87\%
 \end{aligned}
 \tag{34}$$

$$\begin{aligned}
 CI &= 0.24289 + 0.00108 \times WF - 0.02592 \times V + 0.00899 \times WS + 0.02696 \times CT \\
 &\quad - 0.00490 \times V^2 + 0.00549 \times CT^2 - 0.00909 \times WF \times V \\
 R^2 &= 95.79\% \\
 R^2_{adj} &= 94.51\%
 \end{aligned}
 \tag{35}$$

$$\begin{aligned}
 PI &= 0.25706 + 0.01922 \times WF + 0.01921 \times V + 0.01471 \times WS - 0.03793 \times CT \\
 &\quad - 0.01849 \times WS^2 + 0.01193 \times WF \times WS - 0.01572 \times WF \times CT \\
 R^2 &= 88.64\% \\
 R^2_{adj} &= 85.18\%
 \end{aligned}
 \tag{36}$$

D. Poisson models for the residuals

The residuals from the models of the original variables were stored, and the squared residuals were modeled using Poisson regression, obtaining full quadratic models for the residuals.

Once it was possible to obtain the fitted value of the residuals, the weights $W = 1/\hat{\epsilon}_i^2$ were easily obtained and used in the weighted Poisson regression to model the mean of the original variables. The link function was the log link function ($\mu_i = e^{x_i^T \beta}$). The models for the original variables estimated by Poisson regression can be viewed in Eqs. (37)–(40).

E. Poisson models for original variables

$$\begin{aligned}
 D &= \exp(Y'_D) \\
 Y'_D &= -1.1642 - 0.0059 \times WF + 0.0931 \times V + 0.1203 \times WS - 0.1526 \times CT \\
 &\quad + 0.0006 \times WF^2 - 0.0326 \times V^2 - 0.0609 \times WS^2 - 0.0117 \times CT^2 \\
 &\quad + 0.0174 \times WF \times V + 0.0001 \times WF \times ES - 0.0069 \times WF \times CT + 0.0017 \times V \times WS \\
 &\quad + 0.0049 \times V \times CT - 0.0144 \times WS \times CT \\
 R^2 &= 99.37\% \\
 R^2_{adj} &= 99.26\%
 \end{aligned}
 \tag{37}$$

$$\begin{aligned}
 Y &= \exp(Y'_Y) \\
 Y'_Y &= -0.0794 - 0.0057 \times WF - 0.0022 \times V + 0.0075 \times WS - 0.0107 \times CT \\
 &\quad + 0.0048 \times WF^2 - 0.0063 \times V^2 - 0.0021 \times WS^2 - 0.0063 \times CT^2 \\
 &\quad + 0.0011 \times WF \times V + 0.0019 \times WF \times WS - 0.0046 \times WF \times CT + 0.0051 \times V \times WS \\
 &\quad + 0.0054 \times V \times CT - 0.0064 \times WS \times CT \\
 R^2 &= 98.35\% \\
 R^2_{adj} &= 97.12\%
 \end{aligned}
 \tag{38}$$

$$\begin{aligned}
 CI &= \exp(Y'_{CI}) \\
 Y'_{CI} &= -1.4186 + 0.0040 \times WF - 0.1033 \times V + 0.0329 \times WS + 0.1100 \times CT \\
 &+ 0.0028 \times WF^2 + 0.0161 \times V^2 + 0.0045 \times WS^2 - 0.0117 \times CT^2 \\
 &+ 0.0356 \times WF \times V - 0.0065 \times WF \times WS - 0.0033 \times WF \times CT + 0.0064 \times V \times WS \\
 &+ 0.0125 \times V \times CT - 0.0001 \times WS \times CT \\
 R^2 &= 99.90\% \\
 R^2_{adj} &= 99.88\%
 \end{aligned}
 \tag{39}$$

$$\begin{aligned}
 PI &= \exp(Y'_{PI}) \\
 Y'_{PI} &= -1.3665 + 0.0855 \times WF + 0.0767 \times V + 0.0907 \times WS - 0.1665 \times CT \\
 &+ 0.0076 \times WF^2 + 0.0065 \times V^2 - 0.0866 \times WS^2 - 0.0018 \times CT^2 \\
 &+ 0.0038 \times WF \times V + 0.0730 \times WF \times WS - 0.0692 \times WF \times CT - 0.0180 \times V \times WS \\
 &+ 0.0017 \times V \times CT - 0.0308 \times WS \times CT \\
 R^2 &= 98.33\% \\
 R^2_{adj} &= 98.17\%
 \end{aligned}
 \tag{40}$$

F. Individual optimization

The next step is to calculate the individual targets for each variable considering the models constructed through Poisson regression. The payoff matrix obtained is shown in Table 6, where each line represents a variable and in the main diagonal (in bold) are the individual optimum values for each one of them.

G. Multivariate analysis

In a multivariate problem, the variables vary together; thus, it is necessary to consider the correlation within each pair of variables as constraints to the multiobjective problem. Initially, an ellipse for each of these pairs was constructed considering the mean values of the variables and the original data as depicted in Figs. 5, 6, 7, and 8 considering the significance level α equal to 5%.

The red lines in the ellipses represent the multivariate confidence intervals of Bonferroni.

H. Payoff adaptation

Table 6 First payoff matrix

Response	Payoff matrix			
<i>D</i>	0.1760	0.2637	0.3702	0.1788
<i>Rend</i>	0.8916	0.9511	0.8824	0.8935
<i>IC</i>	0.2823	0.2998	0.1808	0.2748
<i>IP</i>	0.1317	0.1915	0.3581	0.1287

The individual variables were optimized one more time, but now Bonferroni’s intervals were used as constraints. An elliptical inequality was also used as constraint in order to consider the multivariate aspect of the problem according to Eq. (41).

$$(\hat{Y} - M)^T \Sigma^{-1} (\hat{Y} - M) \leq \chi^2_{1-\alpha, p}
 \tag{41}$$

where \hat{Y} is the vector of estimated values for the investigated variables, M is the vector of mean values, Σ^{-1} is the inverse of the variance-covariance matrix of the data, and finally $\chi^2_{1-\alpha, p}$ represents a value which results in the probability 100(1- α)% to a chi-square distribution with p degrees of freedom. The current payoff matrix, after adding the aforementioned constraints, is depicted in Table 7.

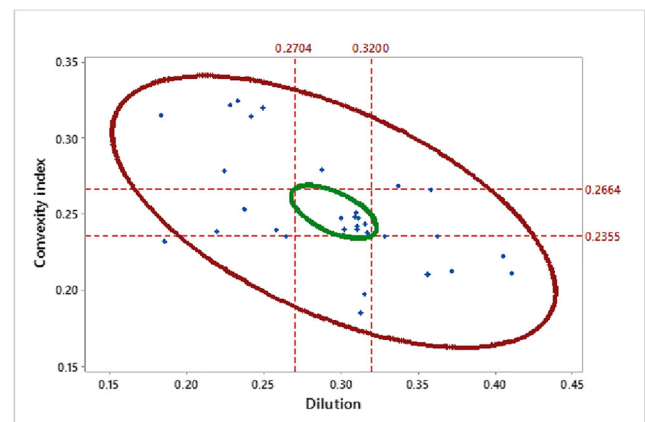


Fig. 5 Ellipse for the data in red, ellipse for the mean in green, and Bonferroni intervals for *CI* and *D* with $\alpha = 5\%$

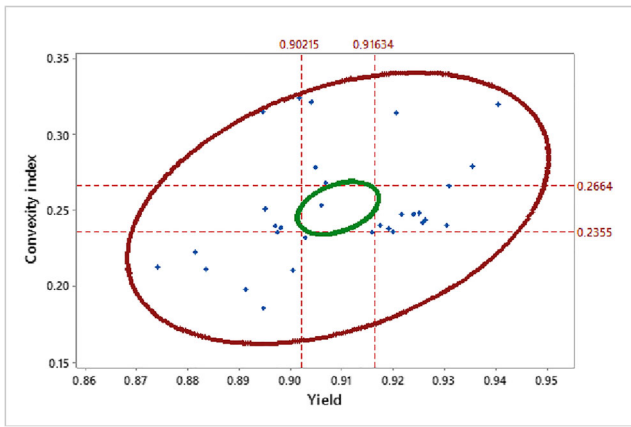


Fig. 6 Ellipse for the data in red, ellipse for the mean in green, and Bonferroni intervals for *CI* and *Y* with $\alpha = 5\%$

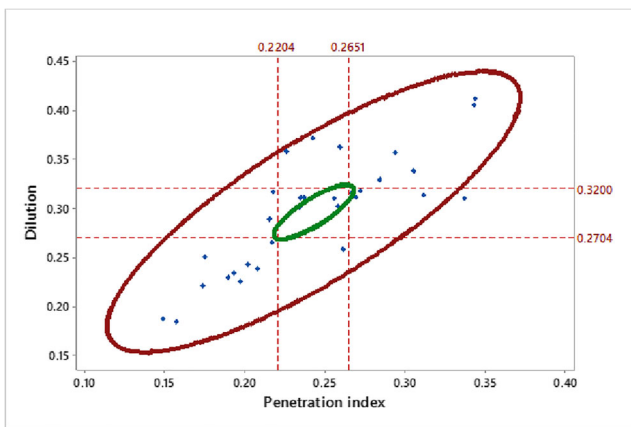


Fig. 7 Ellipse for the data in red, ellipse for the mean in green, and Bonferroni intervals for *D* and *PI* with $\alpha = 5\%$

From this matrix, it is possible to obtain the vector of individual optimal values $\phi^T = [0.2704, 0.9163, 0.2355, 0.2204]$.

I. Multiobjective optimization

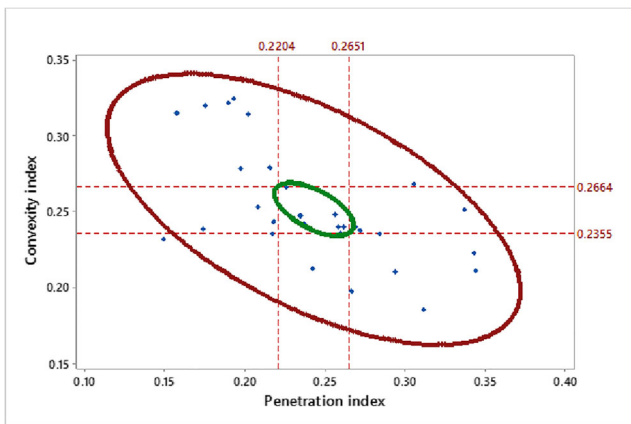


Fig. 8 Ellipse for the data in red, ellipse for the mean in green, and Bonferroni intervals for *CI* and *PI* with $\alpha = 5\%$

Table 7 Updated payoff matrix

Response	Payoff matrix			
<i>D</i>	0.2704	0.3078	0.3049	0.2704
<i>Y</i>	0.9119	0.9163	0.9158	0.9163
<i>CI</i>	0.2440	0.2357	0.2355	0.2355
<i>PI</i>	0.2329	0.2651	0.2637	0.2204

After this, it is necessary to calculate the $FMSE_i$ functions according to Eq. (28) previously presented. The factor models, as previously shown in Eq. (31) and Eq. (32), were obtained through OLS algorithm. The targets for *F1* and *F2* were respectively equal to 0.5216 and 0.2939 after solving Eq. (29). It is important to highlight that the targets for the original variables were extracted from the updated payoff matrix. In this sense, the multiobjective problem was solved using the NBI method. Table 8 shows the optimal values for each NBI subproblem varying the weight (β) from Eq. (7).

Figure 9 depicts the Pareto frontier for the problem.

Table 9 presents the uncoded values for the input factors related to each NBI subproblem.

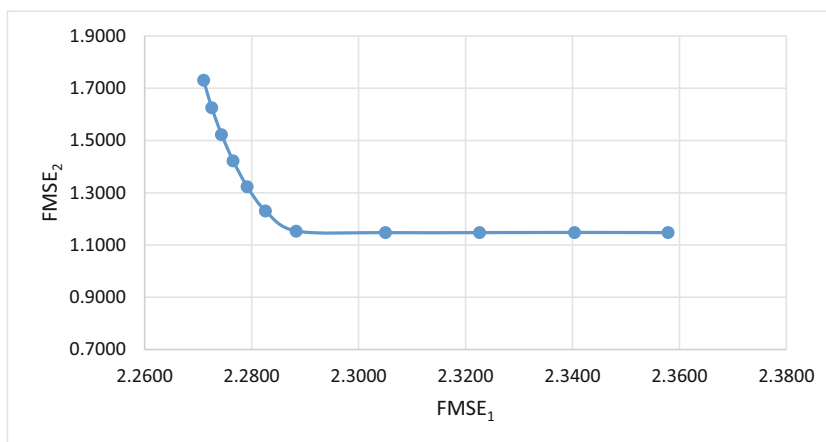
6 Conclusions

The presented paper aimed to explore a new methodology applied in a cladding process of ABNT 1020 carbon steel plate using austenitic ABNT 316L stainless steel cored wire. Poisson regression was applied to generate the mathematical models for the investigated responses dilution, yield, penetration index, and convexity index, in terms of the input variables wire feed rate, arc voltage, welding speed, and contact tip to the workpiece distance.

Table 8 Optimal values for the original variables

<i>B</i>	$FMSE_1$	$FMSE_2$	<i>D</i>	<i>Y</i>	<i>CI</i>	<i>PI</i>
0.00	2.3579	1.1475	0.2848	0.9023	0.2355	0.2651
0.10	2.3404	1.1482	0.2910	0.9021	0.2355	0.2651
0.20	2.3227	1.1475	0.2889	0.9060	0.2355	0.2651
0.30	2.3051	1.1475	0.2963	0.9069	0.2355	0.2651
0.40	2.2884	1.1535	0.3057	0.9080	0.2355	0.2651
0.50	2.2826	1.2309	0.3082	0.9113	0.2355	0.2651
0.60	2.2792	1.3238	0.3100	0.9133	0.2355	0.2651
0.70	2.2766	1.4218	0.3117	0.9148	0.2355	0.2651
0.80	2.2744	1.5228	0.3135	0.9161	0.2355	0.2651
0.90	2.2725	1.6259	0.3171	0.9163	0.2355	0.2651
1.00	2.2710	1.7312	0.3200	0.9163	0.2367	0.2651

Fig. 9 Pareto frontier obtained from the methodology proposed in this paper



The results were satisfactory since accurate models with high values for R^2 and $R^2_{adjusted}$ were achieved. The new constraints were added to the multiobjective optimization problem since they guarantee that the experimenter will consider the simultaneous variation among the variables. By using traditional methods, the researcher may obtain values for the response variables that, although possible to occur individually, would not be feasible in practice. Once the covariance between the variables is not considered, the multivariate nature of the problem is neglected which may incur in erroneous conclusions.

The NBI method produced a set of viable configurations for the input variables that allows the experimenter to encounter the best system setup regarding the importance level of each response. It is important to highlight that the solutions are feasible and non-dominated which means that they represent the best possible scenarios considering all the constraints.

Table 9 Uncoded values for the considered parameters

Weight	WF	V	WS	CT
0	9.757359	28.40929	30.92634	15.90615
0.1	10.03211	28.78429	31.75779	16.92621
0.2	10.24942	29.19409	32.98967	18.04457
0.3	10.47493	29.98383	35.58317	20.05088
0.4	10.37579	32.09922	42.12167	23.62553
0.5	10.05915	32.20054	42.49039	23.48546
0.6	7.990043	27.67858	37.14363	14.81382
0.7	8.083082	27.93774	37.40838	15.4758
0.8	8.166498	28.17388	37.65404	16.04772
0.9	8.248185	28.409	37.90491	16.59043
1	8.332757	28.65724	38.17866	17.13703

Acknowledgments The authors would like to thank the Brazilian agencies of CAPES, CNPq, and FAPEMIG for supporting this research.

Authors' contributions JHG, APP, and PPB: resources; JHG, APP, ERL, SCS, ELR, and PPB: investigation; ERL, ELR, and SCS: data curation; SCS, ELR, and ERL: writing—original draft preparation; ELR, SCS, and ERL: writing—review and editing; JHG, APP, ERL, SCS, ELR, and PPB: visualization; APP, PPB, and JHG: supervision. All of the authors have read and agreed to publish this version of the manuscript.

Data availability All the data used in this research were extracted from [22].

Compliance with ethical standards

Conflict of interest The authors declare that they have no conflict of interest.

Ethical approval Not applicable.

Consent to participate Not applicable.

Consent for publication Not applicable.

References

1. Pessoa ARP (2010) Seleção de parâmetros através do método Taguchi para soldagem de revestimento com ligas de níquel pelo processo MIG/MAG. Soldag. insp. (Impr.), São Paulo. 15(4): 317–324
2. Murugan N, Parmar RS (1997) Stainless steel cladding deposited by automatic gas metal arc welding. Weld J 76:391s–403s
3. Gupta D, Sharma A (2011) Development and microstructural characterization of microwave cladding on austenitic stainless steel. Surf Claddings Technol, Elsevier 205(21–22):5147–5155
4. Phillips AL (1965b) Welding handbook: special welding processes and cutting, vol 3. American Welding Society, London, p 4
5. Marques PV, Modenesi PJ, Bracarense AQ (2005) Soldagem: fundamentos e tecnologia. Belo Horizonte, UFMG, p 362

6. Murugan N, Parmar RS (1994) Effects of MIG process parameters on the geometry of the bead in the automatic surfacing of stainless steel. *J Mater Process Technol* 41(4):381–398
7. Zhang P, Liu Z (2017) On sustainable manufacturing of Cr-Ni alloy claddings by laser cladding and high-efficiency turning process chain and consequent corrosion resistance. *J Clean Prod*, Elsevier 161:676–687
8. Flandinet L, Tedjar F, Ghetta V, Fouletier J (2012) Metals recovering from waste printed circuit boards (WPCBs) using molten salts. *J Hazard Mater* 213–214:485–490
9. Peng S, Li T, Li M, Guo Y, Shi J, Tan GZ, Zhang H (2019) An integrated decision model of restoring technologies selection for engine remanufacturing practice. *J Clean Prod*, Elsevier 206:598–610
10. Palani PK, Murugan N (2006) Development of mathematical models for prediction of weld bead geometry in cladding by flux cored arc welding. *Int J Adv Manuf Technol* 30(7–8):669–676
11. Palani PK, Murugan N (2007) Optimization of weld bead geometry for stainless steel claddings deposited by FCAW. *J Mater Process Technol* 190(1–3):291–299
12. Kannan T, Murugan N (2006) Effect of flux cored arc welding process parameters on duplex stainless steel clad quality. *J Mater Process Technol* 176(1–3):230–239
13. Dupont JN, Marder AR (1996) Dilution in single pass arc welds. *Metall Mater Trans B* 27(3):481–489
14. Banovic SW, Dupont JN, Marder AR (2002) Dilution and microsegregation in dissimilar metal welds between super austenitic stainless steel and nickel base alloys. *Sci Technol Weld Join* 7(6):374–383. <https://doi.org/10.1179/136217102225006804>
15. Gittos MF, Gooch TG (1996) Effect of iron dilution on corrosion resistance of Ni-Cr-Mo alloy cladding. *Br Corros J UK* 31(4):309–314. <https://doi.org/10.1179/bcj.1996.31.4.309>
16. Shahi AS, Pandey S (2006) Prediction of dilution in GMA and UGMA stainless steel single layer cladding using response surface methodology. *Sci Technol Weld Join* 11(6):634–640
17. Balasubramanian V, Lakshminarayanan AK, Varahamoorthy R, Babu S (2009) Application of response surface methodology to prediction of dilution in plasma transferred arc hardfacing of stainless steel on carbon steel. *Int J Iron Steel Res* 16(1):44–53
18. Shahi AS, Pandey S (2008) Modelling of the effects of welding conditions on dilution of stainless steel claddings produced by gas metal arc welding procedures. *J Mater Process Technol* 196(1–3):339–344
19. Black JT, Hunter SL (2003) *Lean manufacturing and cell design*. Society of Manufacturing Engineers, Chicago
20. Piercy N, Rich N (2009) Lean transformation in the pure service environment: the case of the call service centre. *Int J Oper Prod Manag* 29(1):54–76
21. de Almeida FA, Santos ACO, de Paiva AP, Gomes GF, Gomes JHF (2020) Multivariate Taguchi loss function optimization based on principal components analysis and normal boundary intersection. *Eng Comput*, Springer. <https://doi.org/10.1007/s00366-020-01122-8>
22. Gomes JHF, Paiva AP, Costa SC, Balestrassi PP, Paiva EJ (2013) Weighted multivariate mean square error for processes optimization: a case study on flux-cored arc welding for stainless steel claddings. *Eur J Oper Res*, Elsevier 226:522–535
23. de Freitas GJH et al (2011). Otimização de múltiplos objetivos na soldagem de revestimento de chapas de aço carbono ABNT 1020 utilizando arame tubular inoxidável austenítico. *Soldag. insp. (Impr.)*, São Paulo 16(3):232–342
24. Jeffus L (2004) *Welding: principles and applications*, 5th edn. Delmar Learning, Australia, p 904
25. Rodrigues LO, Paiva AP, Costa SC (2008) Otimização do processo de soldagem com eletrodo tubular através da análise da geometria do cordão de solda. *Soldagem & Inspeção* 13(2):118–127
26. Paiva EJ, Rodrigues LO, Costa SC, Paiva AP, Balestrassi PP (2010) Otimização do processo de soldagem FCAW usando o Erro Quadrático Médio Multivariado. *Soldag insp* 15(1):31–40
27. Bryman A (1989) *Research methods and organization studies (contemporary social research)*, 1st edn. Routledge, London
28. Valdenebro, Meseguer JL, Portolés A, Conesa E (2018) Electrical parameters optimisation on welding geometry in the 6063-T alloy using the Taguchi methods. *Int J Adv Manuf Technol* 98:2449–2460
29. Braguine TB, DE Alcântara DS, Castro CAC, DOS Santos GHR (2018) Influence of welding parameters on aluminum tubes AA6063 by the CDFW process | [Influência dos parâmetros de soldagem em tubos de alumínio AA6063 pelo processo CDFW]. *Soldag insp* 23(1):3–16
30. Valdenebro, Meseguer JL, Portolés E, Oñoro J (2016) Numerical study of TTP curves upon welding of 6063-T5 aluminium alloy and optimization of welding process parameters by Taguchi's method. *Indian J Eng Mater Sci* 23:341–348
31. Costa DMD, Brito TG, Paiva AP, Leme RC, Balestrassi PP (2016) A normal boundary intersection with multivariate mean square error approach for dry end milling process optimization of the AISI 1045 steel. *J Clean Prod* 135:1658–1672
32. Montgomery DC (2013) *Design and analysis of experiments*, 8th. edn [S.I.]. John Wiley & Sons, Inc, Hoboken
33. Singh D, Rao PV (2007) A surface roughness prediction model for hard turning process. *Int J Adv Manuf Technol*, Springer 32:1115–1124
34. Myers RH, Montgomery D (2002) *Response surface methodology: process and product optimization using designed experiments*, 2nd edn. [S.I.]. John Wiley & Sons, Inc, Hoboken
35. Torres AF, Rocha FB, Almeida FA, Gomes JHF, Paiva AP, Balestrassi PP (2020) Multivariate stochastic optimization approach applied in a flux-cored arc welding process. *IEEE Access* 8:61267–61276
36. Lu Y, Xu Z (2017) Recycling non-leaching gold from gold-plated memory cards: parameters optimization, experimental verification, and mechanism analysis. *J Clean Prod*, Elsevier 162:1518–1526
37. Nasiri R, Arsalani N (2018) Synthesis and application of 3D graphene nanocomposite for the removal of cationic dyes from aqueous solutions: response surface methodology design. *J Clean Prod*, Elsevier 190:63–71
38. Almeida FA, Gomes GF, Paula VR, Corrêa JE, Paiva AP, Gomes JHF, Turriani JB et al (2018) A weighted mean square error approach to the robust optimization of the surface roughness in an AISI 12L14 free-machining steel-turning process. *J Mech Eng, Strojniški vestnik* 64(3):147–156
39. Myers RH, Montgomery DC, Anderson-Cook CM (2009) *Response surface methodology: process and product optimization using designed experiments*, 3rd edn. Wiley, New York
40. Gaudêncio JHD, Almeida FA, Turriani JB, Quinino RC, Balestrassi PP, Paiva AP (2019) A multiobjective optimization model for machining quality in the AISI 12L14 steel turning process using fuzzy multivariate mean square error. *Precis Eng*, Elsevier 56:303–320
41. Belinato G, Almeida FA, Paiva AP, Gomes JHF, Balestrassi PP, Rosa PARC (2019) A multivariate normal boundary intersection PCA-based approach to reduce dimensionality in optimization problems for LBM process. *Eng Comput*, Springer 35:1533–1544
42. Das I, Dennis JE (1998) Normal-boundary intersection: a new method for generating the Pareto surface in nonlinear multicriteria optimization problems. *SIAM J Optim* 8:631–657
43. Oujebbour F, Habbal A, Ellaia R (2013) Optimization of concurrent criteria in the stamping process. In: *Proceedings of 2013 International Conference on Industrial Engineering and Systems Management (IESM)*, Rabat, pp 1–10

44. Moura D, Barcelos V, Samanamud GRL, França AB, Lofrano R, Loures CCA, Naves LLR, Amaral MS, Naves FL (2018) Normal boundary intersection applied as multivariate and multiobjective optimization in the treatment of amoxicillin synthetic solution. *Environ Monit Assess* 190(3):140
45. Naves FL, de Paula TI, Balestrassi PP, Braga WLM, Sawhney RS, de Paiva AP (2017) Multivariate normal boundary intersection based on rotated factor scores: a multiobjective optimization method for methyl orange treatment. *J Clean Prod Elsevier* 143:413–439
46. Myers RH, Montgomery DC, Vining GG, Robinson TJ (2010) *Generalized linear models with applications in engineering and the sciences*
47. Johnson RA, Wichern DW (2007) *Applied multivariate statistical analysis*, 6th edn. Prentice Hall, Upper Saddle River
48. Hair JF, Black WC, Babin BJ, Anderson RE, Tatham RL (2006) *Multivariate data analysis* 6th Edition. Pearson Prentice Hall, Upper Saddle River
49. King G How not to lie with statistics [Online] Available in <<https://gking.harvard.edu/files/mist.pdf>>: Access in: [August 23, 2020]
50. Paiva AP, Paiva EJ, Ferreira JR, Balestrassi PP, Costa SC (2009) A multivariate mean square error optimization of AISI 52100 hardened steel turning. *Int J Adv Manuf Technol* 43:631–643

Publisher's note Springer Nature remains neutral with regard to jurisdictional claims in published maps and institutional affiliations.